Afyon Kocatepe Üniversitesi Fen ve Mühendislik Bilimleri Dergisi

Afyon Kocatepe University Journal of Science and Engineering

AKÜ FEMÜBİD **23** (2023) 015902 (247-259) AKU J. Sci. Eng. **23** (2023) 015902 (247-259)

DOI: 10.35414/akufemubid.1106218

Araştırma Makalesi / Research Article

Accurate Prediction of Residual Stresses in Machining of Inconel 718 Alloy through Crystal Plasticity Modelling

Sinan KESRİKLİOĞLU [1], Mehmet Fazıl KAPÇI [1], Rıdvan BÜYÜKÇAPAR[1], Barış ÇETİN[2], Okan Deniz YILMAZ[3,4], Burak BAL [1*]

[1] Abdullah Gül University, Department of Mechanical Engineering, Abdullah Gül University, Kayseri.

[2] FNSS Defense Systems Co. Inc., R&D Center, Ankara.

[3] Atılım University, Department of Mechanical Engineering, Ankara.

[4] TRMOTOR Inc., Structural Analysis& Integrity Department, Ankara.

**Corresponding author e-mail: burak.bal@agu.edu.tr. ORCID ID: http://orcid.org/ 0000-0002-7389-9155*

sinan.kesriklioglu@agu.edu.tr. ORCID ID: http://orcid.org/0000-0002-2914-808X

mehmetfazil.kapci@agu.edu.tr. ORCID ID: http://orcid.org/ 0000-0003-3297-5307

ridvan.buyukcapar@agu.edu.tr. ORCID ID: http://orcid.org/ 0000-0002-2550-7911

cetin.baris@fnss.com.tr. ORCID ID: http://orcid.org/ 0000-0001-8615-8383

okan.yilmaz@atilim.edu.tr. ORCID ID: http://orcid.org/ 0000-0002-5431-4334

Geliş Tarihi: 20.04.2022 Kabul Tarihi: 25.01.2023

Abstract

Determination and assessment of residual stresses are crucial to prevent the failure of the components used in defense, aerospace and automotive industries. The objective of this study is to present a material method to accurately predict the residual stresses induced during machining of Inconel 718. Orthogonal cutting tests were performed at various cutting speeds and feeds, and the residual stresses after machining of Inconel 718 were characterized by X-ray diffraction. A viscoplastic self-consistent crystal plasticity model was developed to import the microstructural inputs of this superalloy into a commercially available finite element software (Deform 2D). In addition, same simulations were carried out with classical Johnson - Cook material model. The simulation and experimental results showed that the crystal plasticity based multi-scale and multi-axial material model significantly improved the prediction accuracy of machining induced residual stresses of Inconel 718 when compared to the existing model, and it can be used to minimize the surface defects and cost of production trials in machining of difficult-to-cut materials.

Keywords
Machining; Inconel 718; Crystal Plasticity; Turning; Deform 2D

Kristal Plastisite Modellemesi ile Inconel 718 Alaşımının İşlenmesinde Artık Gerilmelerin Doğru Tahmini

Öz

Artık gerilmelerin belirlenmesi ve değerlendirilmesi, savunma, havacılık ve otomotiv endüstrilerinde kullanılan bileşenlerin arızalanmasını önlemede çok önemlidir. Bu çalışmanın amacı, Inconel 718'in işlenmesi sırasında oluşan artık gerilmeleri doğru bir şekilde tahmin etmek için bir malzeme modeli sunmaktır. Ortogonal talaşlı imalat testleri, çeşitli kesme ve ilerleme hızlarında gerçekleştirilerek, Inconel 718'in işlenmesinden sonraki artık gerilmeler, X-Ray ışın kırınımı ile karakterize edildi. Bu süper alaşımın mikroyapısal girdilerini ticari olarak temin edilebilen bir sonlu eleman yazılımına (Deform 2D) aktarmak için bir viskoplastik kendi içinde tutarlı kristal plastisite modeli geliştirildi. Ayrıca simülasyonlar klasik Johnson - Cook malzeme modeli ile aynı işleme parametrelerinde yapıldı. Bu çalışmada elde edilen simülasyon ve deneysel sonuçlar, kristal plastisite tabanlı çok ölçekli ve çok ölçekli malzeme modelinin, mevcut modele kıyasla Inconel 718'in işleme kaynaklı kalıntı gerilmelerinin tahmin doğruluğunu önemli ölçüde geliştirdiğini ve yüzey kusurlarını en aza indirmek için kullanılabileceğini göstermiştir. Geliştirilen bu model, kesilmesi zor malzemelerin işlenmesinde yüzey kusurlarını ve üretim denemelerinin maliyetini en aza indirmek için kullanılabilir.

Anahtar kelimeler
Talaşlı Üretim; Inconel 718; Kristal Plastisite; Tornalama; Deform 2D

1. Introduction

Nickel-based super alloys (Inconel 718 etc.) have wide application prospects in the field of aerospace, automotive and defense industries due to their superior mechanical properties, and ability to maintain the mechanical performances at high temperatures (Amato *et al*. 2012). Although Inconel 718 alloy has a relatively high yield strength (700-1200 MPa), tensile strength (900-1600 MPa), corrosion resistance and oxidation resistance, it is one of the difficult to cut materials due to the high strain hardening tendency and high toughness during deformation (Rahman *et al*. 1997). Therefore, it is important to determine the optimum cutting parameters with simulations before machining to reduce the manufacturing cost, avoid the surface defects and assure the surface integrity (e.g., residual stress) requirements for the component performance, longevity, and reliability.

Workpiece materials experience high temperatures during machining due to the severe plastic deformation in the primary shear zone to remove the unwanted materials and produce the desired shape. Static and dynamic recrystallization occurs at elevated temperatures during cutting operations (Jawahir *et al*. 2011). The microstructural changes in the cutting process significantly influence the mechanical performance and quality of machined parts (Rotella *et al*. 2013). Therefore, it is required to include the microstructural features into the machining simulations to accurately predict and evaluate the final performance of the machined components. Residual stress after machining is one of the most significant factors that affect the material performance. In particular, the residual stress achieved by the final machining process has an impact on the surface integrity, fatigue life and several other performance indicators.

Several research efforts have been conducted to enhance the knowledge of the machining induced residual stresses in cutting of Inconel 718 alloy. Since the measurement and modelling of this phenomenon are difficult, the findings of previous studies show significant inconsistencies and even there is a discrepancy in its modes (tensile (Arunachalam *et al*. 2004, Sharman *et al*. 2006) or compressive residual stress (Hua *et al*. 2006)) because the magnitude and type of the residual stresses can change with the workpiece material as well as the cutting parameters and cutting tool geometry. Residual stress of the machined parts can be measured experimentally by X-ray diffraction (Jacobus *et al*. 2000) in combination with the electropolishing process to get more accurate residual stress (Outeiro *et al*. 2006). However, this method is expensive and time consuming to analyze the surfaces for each cutting conditions. Therefore, the experimental results are mostly integrated with analytical-empirical and numerical models or used to validate the simulations. Analytical modelling may show close agreements with the experimental results, but it is difficult to apply for all workpiece materials due to the simplifying assumptions. Liang and Su (2007) developed an analytical model to predict the surface and subsurface residual stress profiles in orthogonal machining. Cutting tests were performed to validate the model under various cutting conditions of steel workpieces. Agrawal and Joshi (2013) predicted the residual stresses in orthogonal machining of AISI 4340 steel with an analytical model based on the contact stress in the machining zone and cutting temperature. In their study, the plastic stresses were evaluated by two algorithms because the accuracy of hybrid algorithms is better for low feed rates when compared to the S-J model. An analytical elasto-plastic model and a relaxation procedure (Ulutan *et al*. 2007) were also used to estimate the residual stresses with the thermal field of workpiece and cutting forces acting on the workpiece during the machining operation, and reduce the simulation time. However, the agreement of the model decreases with experimental data for the residual stresses when approaching the machined surfaces.

With the advances in the computer technologies and numerical models, finite element (FE) simulations are also combined with constitutive material models to predict the machining induced residual stresses. Although many material models were developed for the elastic and thermal properties of Inconel 718, Johnson - Cook plasticity model (1983) including the hardening law and hardening rate as well as the thermal softening is

widely used to simulate the machining operation. Outerio *et al*. (2008) developed a three-dimensional finite element model to investigate the residual stresses on the machined and sub-surfaces. The simulation and experimental results showed that high tensile stresses occur on the machined surface while compressive residual stresses exist in the subsurface. It was also found that coating of the cutting tools causes high tensile stresses on the machined surface for Inconel 718 alloy and AISI 316L steel. Salio *et al*. (2006) predicted the residual stresses in orthogonal machining of Inconel 718 with an implicit FE model based on the updated Lagrangian formulation (Strenkowski and Carroll, 1985), and compared the simulation results with analytical models and experimental measurements. In that model, the residual stress results were in a good agreement within the 100 µm from the machined surface when assumed a rigid plastic constitutive law. Torrano *et al*. (2011) presented an explicit finite element code in Abaqus for a turning operation of Inconel 718 and compared the residual stress predictions with other two commercially available software (Deform and AdvantEdge) since different material behavior laws are used in these programs. All three simulations showed that only qualitative information can be obtained about the machining induced residual stresses with finite element models. Jawahir *et al*. (2011) concluded that the magnitude of the predicted residual stresses deviate significantly for different workpiece materials although the cutting temperatures, forces and chip compression ratio are similar, and the uncertainty can be as large as 160% with the same material model used to simulate the machining of steels and Inconel 718 (Kortabarria *et al*. 2016).

The numerical simulations mentioned above showed that the material constitutive laws are critical to establish a finite element model of the machining process, and important to accurately predict the machining induced residual stresses. Therefore, several material models were used to simulate the plastic deformation during cutting operation. In the THAN material constitutive model (Calamaz *et al*. 2008), the strain softening effect is added to the Johnson - Cook (J-C) plasticity model to study the effect of strain softening phenomena as well as temperature and strain dependence of the flow stress. Hollomon's law (Dixit *et al*. 2011) includes the empirically determined hardening parameters and provides a good approximation of plastic deformation although it significantly deviates at low strains. Ludvik's Law (Dixit *et al*. 2011) is a modified version of the Hollomon's law, and also includes the yield strength of the material. Both models are extensively used in the metal forming process. The modified Mohr-Coulomb model Sjöberg *et al*. (2018) was also used to characterize the fracture behavior of Inconel 718 at elevated temperatures. The tensile test performed at various temperatures showed that the strains of this model agree well with the experimental data of Inconel 718. This model was also implemented to the machining prosses by Silva *et al*. (2020) to predict the residual stresses in orthogonal cutting of Inconel 718. Since this model takes into account the effect of strain rate, temperature, stress triaxiality and lode angle, the accuracy was enough to investigate the effects of cutting parameters and tool orientation on the machining induced residual stress.

Earlier studies proved that utilizing viscoplastic self-consistent (VPSC) crystal plasticity model, which covers microstructural changes over classical material models at macroscale, improves the accuracy of the finite element results (Bal, 2018, Onal *et al*. 2015, 2014). In addition, accurate residual stress prediction is of utmost importance for the prevention of manufacturing trials and improve surface integrity and quality. However, to the best of authors' knowledge, a crystal plasticity based material model has never been proposed yet to predict residual stress after machining of Inconel 718. The objective of this work is to present a multiscale modelling approach to accurately quantify the residual stresses induced during orthogonal cutting of Inconel 718. For this purpose, cutting tests were performed at various cutting parameters, the transient force components were measured, and the machining induced residual stresses predicted by VPSC model were compared with the classical Johnson - Cook material model results and X-ray diffraction measurements.

2. Material and Methodology

Orthogonal dry cutting tests were conducted on Inconel 718 alloy by a CNC lathe at various cutting speeds and feeds which were compiled from a machinery handbook. Inconel 718 workpiece was a 50 mm diameter round bar with a chemical composition of Ni (53.89 wt.%), Cr (17.81 wt.%), Mo (2.89 wt.%), Nb (5.10 wt.%), Ti (0.96 wt.%), Al (0.51 wt.%), Fe (Bal.) and the impurity amounts of C, Mn, Si, P, S, Co, Ta, B and Cu. It was also annealed at 954 ^{o}C, quenched in water and aged at 750 ^{o}C for 8 hours by the manufacturer to obtain a hardness of 43 HRC. CVD coated carbide grooving tools (Korloy MGMN300-M - NC3120) were used with a rake and relief angles of 5 degrees, and a cutting-edge radius of 2 µm. The workpiece material was first machined with a turning tool and grooves were then made to obtain 3 mm wide ribs for the orthogonal cutting tests as shown in **Hata! Başvuru kaynağı bulunamadı.**. During the machining, the transient cutting and trust forces were measured by a Kistler force dynamometer, and a multifunction PCI Card was used to acquire the signals at a sampling rate of 1 kHz and convert the voltage inputs into the force. Average steady state forces were calculated in Matlab to compare with the predicted forces of the VPSC and J-C models.

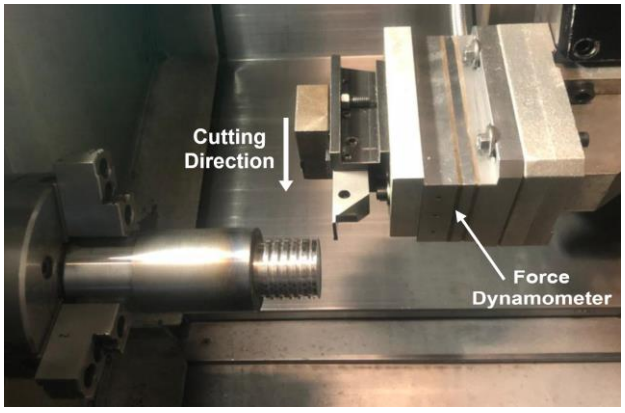

Figure 1. Orthogonal cutting test setup

The residual stresses on the machined surface at different cutting conditions were analyzed by the X-ray diffractometer (Bruker D8 Discover), operating at 40 kV and 40 mA with a Cu-Kα radiation source (wavelength = 1.5406 Å). After all the cutting tests, the workpiece was placed on the Euler Cradle mechanism to orient during measurements. The strains in the crystal lattice of Inconel 718 were first measured on machined surface with various diffraction peaks and then, the $\sin^2\psi$ method Fitzpatrick *et al*. (2005) was used with a limited penetration of X-rays and elastic constants to calculate the machining induced residual stresses as presented in Results and Discussion part.

The mechanical behavior of Inconel 718 was first determined by a uniaxial tensile test using a universal mechanical testing system (Instron 8801) through the ASTM E8/E8M standard (Tadano *et al*. 2012) at ambient temperature and a strain rate of 0.01 s^{-1}. Corresponding mechanical behavior was used to determine the Voce hardening parameters of Inconel 718 via the crystal plasticity simulations discussed in the subsequent section.

Machining process changes the microstructure of workpiece materials in micro and nano scale due to the high strain interactions, strain rates and temperatures. The microstructure and mechanical properties of the machined surface can be controlled with a proper selection of the cutting parameters. In this study, the machining induced residual stresses were predicted and analyzed by a VPSC model to provide a comprehensive understanding of the surface integrity of Inconel 718 parts after machining. Orthogonal turning tests were also performed to validate the reliability of the VPSC model, and the model was compared to the Johnson - Cook constitutive model with respect to the deformation response of the workpiece material.

2.1 Johnson - Cook Plasticity Model

The residual stresses in the orthogonal machining of Inconel 718 were first predicted with the Johnson – Cook (J-C) constitutive model (Johnson and Cook, 1983) to compare with the multi scale material model (VPSC). The J-C model describes the plastic deformation behavior of the workpiece material at large strains, strain rates and high temperatures, but microstructural effects are not included in this material model. The flow stress in the J-C plasticity model is expressed as

$$\sigma_{JC} = (A + B\varepsilon^{n})\left(1 + C\ ln\left(\frac{\dot{\varepsilon}}{\dot{\varepsilon}_o}\right)\right)\left(1 - \left(\frac{T - T_o}{T_m - T_o}\right)^{m}\right) \quad (1)$$

where A is the yield strength, B is the hardening modulus, n is the strain-hardening exponent, C is the strain rate sensitivity, m is the thermal sensitivity, T_m, is the melting temperature, $\dot{\varepsilon}$ is the strain rate, $\dot{\varepsilon}_o$ reference strain rate of the workpiece material and T_o is the ambient temperature. All of the parameters were compiled from (Grzesik *et al*. 2017) and listed in **Table 1**.

Table 1. Johnson - Cook Model Parameters for Inconel 718 (Grzesik *et al*. 2017)

$\boldsymbol{A}$ [MPa]	1012
$\boldsymbol{B}$ [MPa]	511
$\boldsymbol{C}$	0.0271
$\boldsymbol{n}$	0.396
$\boldsymbol{m}$	4.33
$\boldsymbol{T_o}$ [C°]	20
$\boldsymbol{T_m}$ [C°]	1277

The Johnson - Cook material model with Cockcroft Latham fracture criteria was implemented in the Deform 2D finite element software to simulate the cutting process for the same cutting parameters used in the experiments and VPSC model, and estimate the machining induced residual stresses. Critical value of failure criteria was chosen 500 by calculation the area under the stress strain curve through the ultimate tensile strength of the material. The fixed displacement boundary condition was applied to the cutting tool at x and y direction while the workpiece was only fixed at y direction. It is assumed that the small amount of heat transfer occur between the cutting tool and workpiece so the heat transfer coefficient was taken as a 10000 (W/m^2°C).

2.2 Crystal Plasticity Formulation

The viscoplastic self-consistent (VPSC) model written in FORTRAN 77 was utilized to obtain a material model that captures the microstructural features (Lebensohn and Tomé, 1993). In particular, hardening parameters on the slip system level were determined by means of uniaxial stress-strain response (Bal *et al*. 2018, 2016). Equivalent stress-strain responses of Inconel 718 for each cutting speed and feed combinations were then computed using the same hardening parameters and velocity gradients via the finite element modelling software. As the multi axial deformation exists in the orthogonal cutting, crystal plasticity based equivalent stress-strain responses were incorporated in the finite element analysis to achieve more close machining outcomes since the deformation response of the loadings can only be calculated after accurately formulating the process and validating with the experimental data.

Deformation of Inconel 718 was modeled at the microscopic level based on the uniaxial deformation response of the machining process. In this approach, the corresponding resolved shear stress can be defined as

$$\tau_{RSS}^{s} = m_i^s \sigma_i \tag{2}$$

where m_i^s is the Schmid tensor and σ_i is the applied stress in the vector forms for a system (s). The nonlinear shear strain rate can be expressed as

$$\dot{\gamma}^s = \dot{\gamma}_0 \left(\frac{\tau_{RSS}^s}{\tau_0^s}\right)^n = \dot{\gamma}_0 \left(\frac{m_i^s \sigma_i}{\tau_0^s}\right)^n \tag{3}$$

where $\dot{\gamma}_0$ is the reference strain rate, τ_0^s is the threshold stress at a strain rate of $\dot{\gamma}_0$ and n is the inverse of strain rate sensitivity index. The plastic strain rate can be written in a linear form (Lebensohn and Tomé, 1993);

$$\dot{\varepsilon}_k = \left[\dot{\gamma}_0 \sum_1^s \frac{m_i^s m_j^s}{\tau_0^s} \left(\frac{m_k^s \sigma_k}{\tau_0^s}\right)^{n-1}\right] \sigma_j = M_{ij}^{c(sec)}(\tilde{\sigma})\sigma_j \tag{4}$$

where $M_{ij}^{c(sec)}$ is the secant viscoplastic compliance of the crystal by assuming the stress is related to the polycrystal strain rate in each grain. This relation is expressed as (Lebensohn and Tomé, 1993)

$$\dot{E}_i = M_{ij}^{(sec)} \tilde{\Sigma} \Sigma_j + \dot{\Sigma}_0 \tag{5}$$

where Σ denotes the applied stresses. The deviations in the strain rate and stress can be defined as

$$\widetilde{\dot{\varepsilon}_k} = \dot{\varepsilon}_k - \dot{E}_k \tag{6}$$

$$\tilde{\sigma_j} = \sigma_j - \Sigma_j \quad (7)$$

where $\dot{\varepsilon_k}$ and σ_j are the local strain and stress in a single crystal or grain level, respectively. The stress equilibrium can be derived with the Eshelby's inhomogeneous inclusion theory (Eshelby, 2007) as follows (Kocks *et al*. 1998).

$$\tilde{\dot{\varepsilon}} = -\widetilde{M}:\tilde{\sigma} \quad (8)$$

where $\widetilde{M}$ is the interaction tensor defined as

$$\widetilde{M} = n'(I-S)^{-1}:S:M^{(\sec)} \quad (9)$$

where $M^{(\sec)}$ is the polycrystal aggregate compliance tensor, and S is the Eshelby viscoplastic tensor. The macroscopic compliance can be obtained by substituting Equations (3) and (4) into Equation (7).

$$M^{(\sec)} = \langle M^{c(\sec)}:\left(M^{c(\sec)} + \widetilde{M}\right)^{-1}:\left(M^{c(\sec)} + \widetilde{M}\right)\rangle \quad (10)$$

The stresses of each grain at an applied strain rate, crystal's compliance tensor and polycrystal compliance can be calculated by solving the Equations (3), (7) and (9) with an iterative approach. The overall dislocation density rate is defined as (Lebensohn and Tomé, 1993)

$$\dot{\rho} = \sum_n \left\{k_1\sqrt{\rho} - k_2\rho\right\}|\dot{\gamma}^n| \quad (11)$$

where k_1 and k_2 are the geometric constants defined the statistical storage of the moving dislocations (Kocks *et al*. 1998). The flow stress described by the classic Taylor's hardening law is given by

$$\tau = \tau_0 + \alpha\mu b\sqrt{\rho} \quad (12)$$

where α is interaction parameter of the dislocations, μ is the shear modulus of the workpiece and b is the Burgers vector.

From the Equation (11), the flow stress rate can be expressed as

$$\dot{\tau} = \frac{\alpha\mu b\dot{\rho}}{2\sqrt{\rho}} \quad (13)$$

Substituting Equation (10) into Equation (12) leads to

$$\dot{\tau} = \sum_n \left\{k_1\frac{\alpha\mu b}{2} - k_2\frac{\alpha\mu b}{2}\sqrt{\rho}\right\}|\dot{\gamma}^n| \quad (14)$$

When the Equation (12) is rearranged and substituted into the Equation (14), the flow stress evolution rate is obtained;

$$\dot{\tau} = \sum_n \left\{k_1\frac{\alpha\mu b}{2} - k_2\frac{\tau-\tau_0}{2}\right\}|\dot{\gamma}^n| \quad (15)$$

where $\left\{k_1\frac{\alpha\mu b}{2} - k_2\frac{\tau-\tau_0}{2}\right\}$ expresses the linear Voce hardening term. Equation (15) can also be defined as a function of the constant strain hardening rate, θ_0, and saturation stress, τ_s, when the geometric effects and threshold stresses are not available.

$$\dot{\tau} = \sum_n \left\{\theta_0\left(\frac{\tau_s-\tau}{\tau_s-\tau_0}\right)\right\}|\dot{\gamma}^n| \quad (16)$$

In machining operations, the hardening can be defined by the extended Voce law and the threshold stress evolution is given by

$$\tau^s = \tau_0 + (\tau_1 + \theta_1\Gamma)(1 - \exp(-\frac{\theta_0\Gamma}{\tau_1})) \quad (17)$$

where Γ is the accumulated shear strain in the grain, $\theta_1$is the asymptotic hardening, and $\tau_1$is the back-extrapolated critical resolved shear stress.

2.1 Incorporation of the Crystal Plasticity Model into Finite Element Simulations

Random texture was used during the crystal plasticity computations. τ_0 is calculated as the ratio of the experimentally determined yield stress of Inconel 718 to the Taylor factor (3.03 ± 0.3) in multi-grain structures (Tadano *et al*. 2012). Other hardening parameters (τ_1, θ_0 and θ_1) were identified after VPSC computations (Figure 2). It should be noted that 12 primary slip systems used as crystal plasticity inputs were activated in the face centered cubic crystal and the twinning mechanism was neglected since it does not contribute to the deformation during machining (Sui et al., 2021, 2018). VPSC model was used to calculate the equivalent stress-strain response of uniaxial deformation of Inconel 718 (Figure 3). **Hata! Başvuru kaynağı bulunamadı.** shows the comparison of the predicted deformation response and the tensile loading results. As shown in **Hata! Başvuru kaynağı bulunamadı.**, the agreement is nearly exact except for the initial plastic deformation as it is a common observation in the crystal plasticity modelling (Bal, 2018, Bal *et al*.,

2016), and it indicates that the numerical solution is adequate in predicting the stresses during cutting of Inconel 718. The experimental results proved that, the modelling of material deformation has been successfully carried out. Therefore, the VPSC material modelling was used for the prediction of the equivalent stress-strain graph with the same hardening parameters.

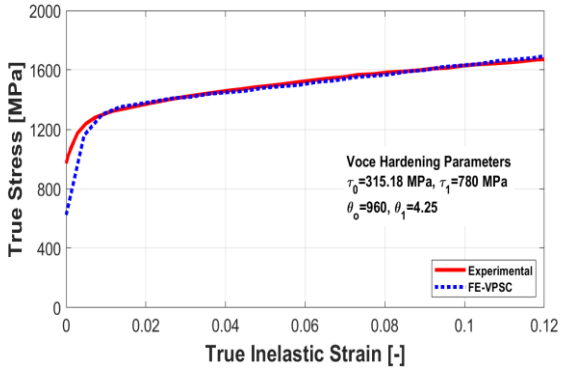

Figure 2. Crystal plasticity modeling of Inconel 718.

The FE mesh was applied to each material to observe the stress strain distribution. Then, the VPSC material modelling was used to predict equivalent stress strain distribution in the plastic region. The velocity gradients for each cutting condition must be obtained to simulate the texture evolution by the VPSC modelling. The same Voce hardening parameters were used in the crystal plasticity based multi scale modelling to control the activation of the slip modes during machining of Inconel 718.

Table 2 shows the velocity gradients for a combination of different cutting speeds and feeds obtained via the Deform 2D software. The usability and validity of this incorporation were utilized successfully before (Onal *et al*. 2015, 2014).

Table 2. Velocity gradient tensors for machining of Inconel 718 at various cutting parameters

Feed [mm/rev]	**Cutting Speed [m/min]**								
	15			**30**			**60**		
0.040	0.84 1 0	1 −0.42 0	0 0 −0.42	0.75 1 0	1 −0.375 0	0 0 −0.375	1.02 1 0	1 −0.51 0	0 0 −0.51
0.050	1.01 1 0	1 −0.505 0	0 0 −0.505	0.27 1 0	1 −0.135 0	0 0 −0.135	0.89 1 0	1 −0.445 0	0 0 −0.445
0.060	0.83 1 0	1 −0.415 0	0 0 −0.415	1.05 1 0	1 −0.525 0	0 0 −0.525	0.43 1 0	1 −0.215 0	0 0 −0.215
0.080	1.11 1 0	1 −0.555 0	0 0 −0.555	1.3 1 0	1 −0.65 0	0 0 −0.65	1.13 1 0	1 −0.565 0	0 0 −0.565
0.090	1.30 1 0	1 −0.65 0	0 0 −0.65	0.83 1 0	1 −0.415 0	0 0 −0.415	1.23 1 0	1 −0.615 0	0 0 −0.615
0.100	1.24 1 0	1 −0.62 0	0 0 −0.62	0.66 1 0	1 −0.33 0	0 0 −0.33	0.91 1 0	1 −0.455 0	0 0 −0.455

The velocity gradients for each cutting speed and feed were computed as show in

Table **2**. **Hata! Başvuru kaynağı bulunamadı.** shows the prediction of equivalent stress- strains with the VPSC simulations. Equivalent stress-strain deformation responses of the machined materials were computed by VPSC using 18 different velocity gradient as an input data to define the plastic flow characteristics of each samples seperately.

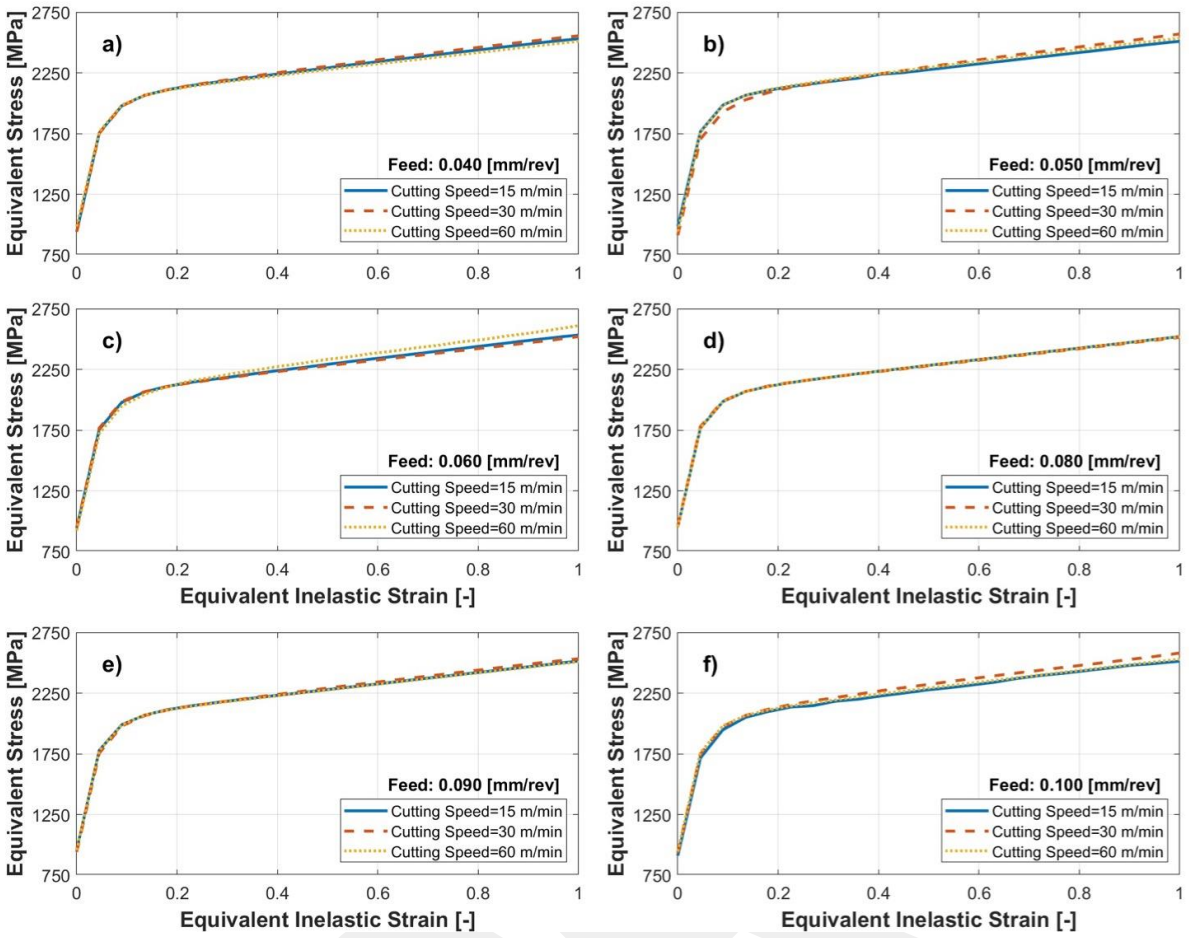

Figure 3. Predicted Equivalent Stresses - Strains for Inconel 718 at the feeds of a) 0.040 mm/rev, b) 0.050 mm/rev, c) 0.060 mm/rev, d) 0.080 mm/rev, e) 0.090 mm/rev and f) 0.100 mm/rev

A commercially available finite element software, STFC Deform 2D, was used to simulate the orthogonal cutting process of Inconel 718 based on the VPSC multiscale material model with Voce hardening law. In the simulations, the workpiece and tool were modeled as an elastic plastic material, and perfectly rigid, respectively. The dimension of the workpiece was the 2 mm x 0.4 mm and cutting tool geometry did not change the all the simulation. Approximately 3000 and 1230 second order quad elements with a minimum size of 0.004 mm and a curvature angle of 30° were placed on the workpiece and cutting tool, respectively. Dynamic meshes were also concentrated in the cutting zone as shown in **Hata! Başvuru kaynağı bulunamadı.** to model chip formation more effectively. **Hata! Başvuru kaynağı bulunamadı.** shows the stresses on the machined surfaces during orthogonal cutting of Inconel 718 at a cutting speed of 30 m/min and feed of 0.09 mm/rev. It should be noted that the residual stresses were extracted after the machining simulation when the workpiece temperature reached to the ambient temperature (20 °C) for all cutting conditions to minimize the effects of cooling on the predictions.

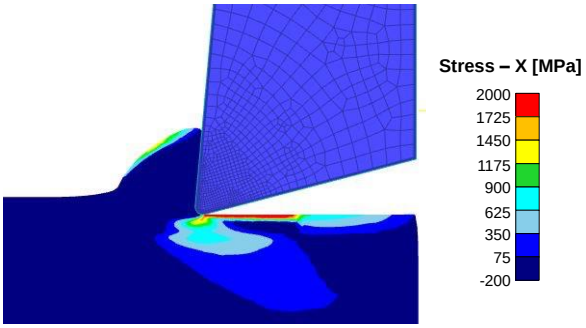

Figure 4. Predicted stresses of VPSC multiscale model on the workpiece during machining of Inconel 718.

3. Results and Discussion

In this section, the influence of cutting parameters on the cutting forces, thrust forces and residual stresses was investigated in machining of Inconel 718 since cutting speeds and feeds are limiting parameters due to the low thermal conductivity, high hardness and high temperature strength. Cutting and thrust forces were first measured during the orthogonal cutting tests and compared to the forces predicted by the multiscale material model and Johnson - Cook (J-C) constitutive model. Comparison between the machining induced residual stresses obtained by the X-ray diffraction technique and estimated by the two models was also presented.

3.1 Effect of Cutting Parameters on Cutting and Thrust Forces

The transient principal forces acting on the cutting tool were measured by a force dynamometer mounted on the tool turret of CNC lathe during all the cutting tests. The predicted and measured average cutting and trust forces were calculated at steady state condition for each cutting parameter and shown in **Hata! Başvuru kaynağı bulunamadı.**. As expected, the increase in the machining forces was fairly linear with the cutting speeds and feeds. Increasing the feed influenced the rate of experimental cutting forces greater than the thrust forces. Although the VPSC model showed the same trends for all cutting conditions studied, the cutting force rate remained almost constant for a cutting speed of 60 m/min in the J-C model predictions. Moreover, the thrust forces predicted by the J-C model were not influenced by the cutting speeds and feeds used in the cutting tests. This might be due to the simplified frictional model with a Coulomb friction coefficient in the J-C material model.

Although the cutting forces (tangential) were greater than the thrust forces at all feeds for a cutting speed of 15 m/min (**Hata! Başvuru kaynağı bulunamadı.**a), increasing the cutting speed led to a reduction in the cutting forces at a feed of 0.04 mm/rev for a cutting speed of 30 mm/min (**Hata! Başvuru kaynağı bulunamadı.**b) and at feeds smaller than 0.08 mm/rev for a cutting speed of 60 m/min (**Hata! Başvuru kaynağı bulunamadı.**c) in orthogonal turning of Inconel 718 with a coated cutting tool. This could be due to the ratio of the cutting-edge radius to the feed rate since the apparent rake angle would be negative for small uncut chip thicknesses and cause an increase in the thrust forces. As can be seen from the **Hata! Başvuru kaynağı bulunamadı.**, the apparent coefficient of friction increases with the feed and cutting speed for the cutting conditions used in the machining tests.

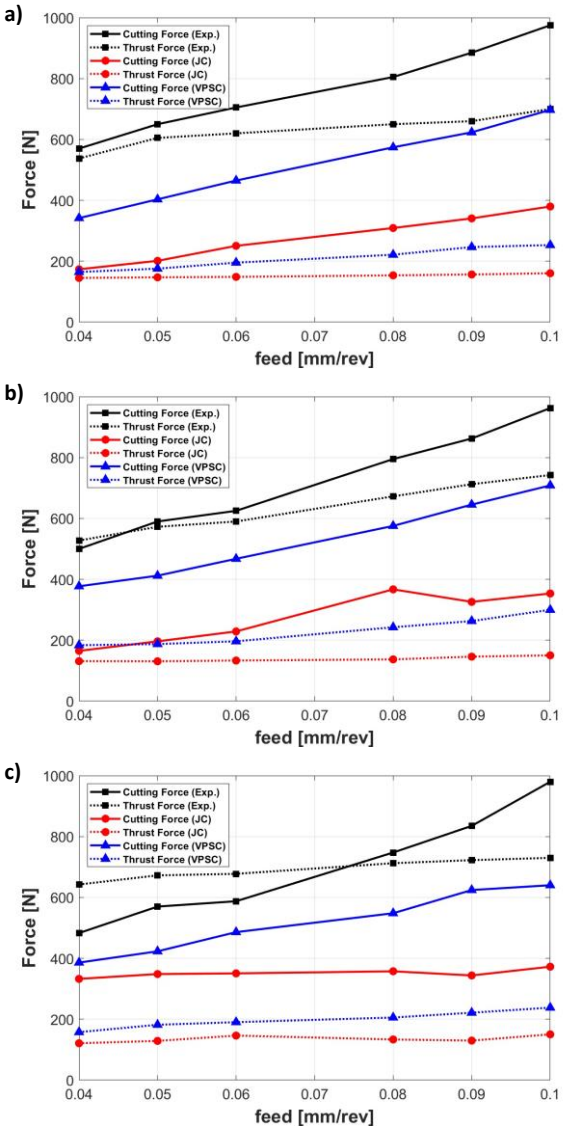

Figure 5. Effect of feeds on the cutting and thrust forces at cutting speeds of (a) 15 m/min, (b) 30 m/min, (c) 60 m/min.

As shown in **Hata! Başvuru kaynağı bulunamadı.**, the influence of feeds on the thrust force reduced significantly with the cutting speed. Thrust force only increased by 82.5 N at a cutting speed of 60

m/min when the feed was changed from 0.04 mm/rev to 0.1 mm/rev. It was also observed that increasing the cutting speed slightly reduce the cutting forces. All the experiments and simulations showed that the VPSC material model can capture the force trends better than the J-C model and it is in closer agreement with the measurement results for all the cutting conditions. This also indicates that the microstructural inputs are indeed the main factors and contribute to the prediction accuracy of the cutting and thrust forces.

3.1 Effect of Cutting Parameters on Residual Stresses

The machining induced residual stresses were first measured by X-ray diffraction (XRD) after each cutting tests as described in the section of Material and Experimental Setup, and shown in **Hata! Başvuru kaynağı bulunamadı.**. The uncertainty in the XRD measurements is due to the variation of diffraction peaks, incident angle and off-axis angle. Within the range of the cutting parameters investigated, it was observed that the residual stresses on the machined surface were mainly tensile due to thermal strain associated with the cutting process. The residual stresses were also obtained from the machined surfaces of the finite element analysis after the cutting simulation was ended and the workpiece temperature were cooled down to the ambient temperature. A line was then placed onto the machined surface to extract the nodal values and the average residual stresses were calculated in Matlab for each cutting parameter. **Hata! Başvuru kaynağı bulunamadı.** shows the machining induced residual stresses as a function of feed at cutting speeds of 15 m/min, 30 m/min and 60 m/min. The machining induces residual stresses decreased significantly for a feed of greater than 0.09 mm/rev, and unlike the J-C constitutive model, the viscoplastic self-consistent (VPSC) model could capture this reduction for all cutting speeds. XRD measurements showed that tensile residual stresses occur in orthogonal machining of Inconel 718 with positive rake angle coated inserts, except for a feed of 0.1 mm/rev at a cutting speed of 15 m/min. Even if the residual stress slightly reduced in the VPSC model at this condition and became less tensile, it was not compressive. On the contrary, the J-C model predicted a sharp increase in the residual stress at this cutting condition.

Although the residual stresses increased with the cutting speeds, there were no significant trends observed regarding the residual stresses with respect to the feeds. Increasing the feed from 0.05 mm/rev to 0.08 mm/rev resulted in a reduction in the residual stress by 14 MPa at a cutting speed of 60 m/min whereas it increased the residual stress by 360 MPa at 30 m/min. The maximum residual stress (870 MPa) was measured at a cutting speed of 60 m/min for a feed of 0.09 mm/rev. Although the same amount of material (120 mm^3/s) was removed at a cutting speed of 30 m/min and a feed of 0.08 mm/rev, and a cutting speed of 60 m/min and a feed of 0.04 mm/rev, the measured tensile residual stress was approximately 320 MPa less at the higher cutting speed condition. Since the thermally dominant deformation contributes to the magnitude of tensile residual stresses (Pawade *et al*. 2008), at high cutting speeds, most of the heat generated during the machining process will be transferred through the chips and the rate of the heat dissipation into the workpiece decreases. This may explain the reduction of residual stress in the tensile direction. It should be noted that the trend of the residual stresses may change with different levels of cutting parameters. Measurement of the cutting edge temperature would be required to investigate the relative importance of the thermal and mechanical effects.

As can be seen from the **Hata! Başvuru kaynağı bulunamadı.**, the agreement between the XRD measurements and VPSC predictions increases with the cutting speeds due to the higher contribution of the thermal strains. Although similar trends were observed between the experimental and numerically predicted results, the experimentally measured residual stresses were lower than the predictions of Johnson - Cook (J-C) constitutive model and viscoplastic self-consistent (VPSC) multiscale material model. The reason for this discrepancy could be due to the nature of X-ray beams because the measurements of residual stresses are averaged from a finite volume of the

workpiece material even if the X-ray beam is focused on the surface of the workpiece material (Noyan and Cohen, 1987), but they were compared with the results extracted from the machined surfaces. Since the magnitude of residual stresses decreases significantly on the subsurface layers (**Hata! Başvuru kaynağı bulunamadı.**), the sublayers contribute to the total diffracted intensity. Therefore, it is expected that the predicted residual stresses will be greater than the XRD measurements. Another possible reason is the inhomogeneous residual stress distributions on the machined surfaces. Nevertheless, the VPSC model improved the prediction accuracy by a maximum of approximately 21% when compared to the J-C material model in orthogonal machining of Inconel 718.

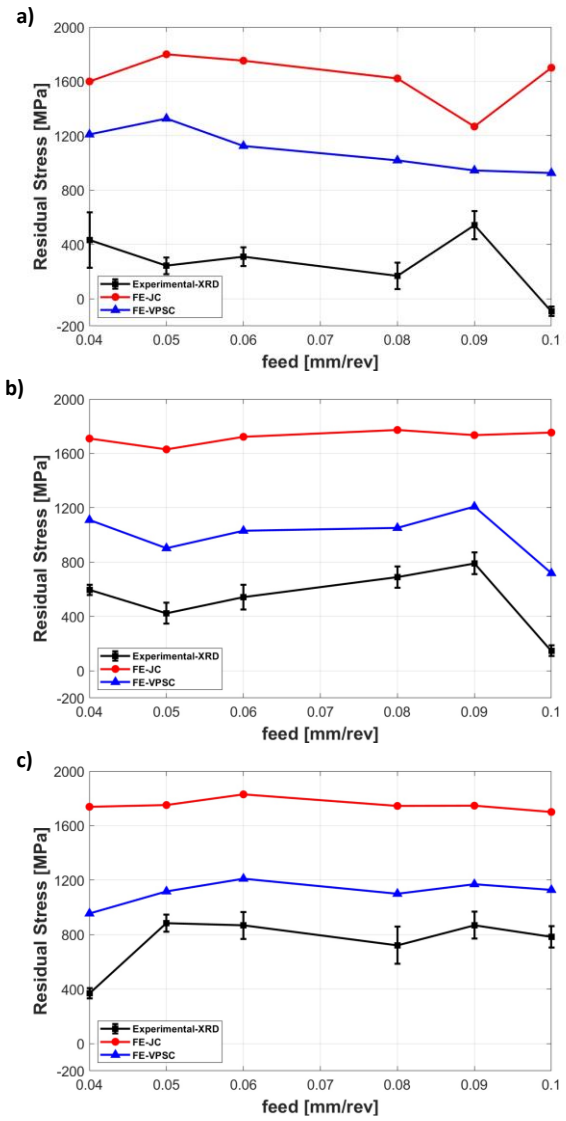

Figure 6. Measured and predicted residual stresses in XX direction at cutting speeds of (a) 15 m/min, (b) 30 m/min, (c) 60 m/min.

4. Conclusion

An unique multiaxial material model was incorporated into machining simulation to obtain more accurate results over classical material model. Orthogonal dry cutting tests were conducted with CVD coated grooving tools, and cutting force components were monitored during each experiment. Residual stresses after each experiment were determined by means of XRD. It was found that the residual stress increases with the cutting speeds although the feed does not have considerably effects on it, and the VPSC model was able to capture the trends of both cutting forces and the residual stresses more precisely in orthogonal cutting of Inconel 718. Overall, the proposed material model can be used in machining simulations to catalyse the selection machining parameters process, improve the surface integrity of the machined part and decrease the cost of whole machining process.

Acknowledgement

B. Bal acknowledges the financial support by the Scientific and Technological Research Council of Turkey (TUBITAK) ARDEB-3001 Initial R&D Projects Support Program under Project no. 118M253.

5. References

Agrawal, S. and Joshi, S.S., 2013. Analytical modelling of residual stresses in orthogonal machining of AISI4340 steel. Journal of Manufacturing Processes, **15**(1), pp.167-179.

Amato, K.N., Gaytan, S.M., Murr, L.E., Martinez, E., Shindo, P.W., Hernandez, J., Collins, S. and Medina, F., 2012. Microstructures and mechanical behavior of Inconel 718 fabricated by selective laser melting. Acta Materialia, **60**(5), pp.2229-2239.

Arunachalam, R.M., Mannan, M.A. and Spowage, A.C., 2004. Residual stress and surface roughness when facing age hardened Inconel 718 with CBN and ceramic cutting tools. International Journal of Machine Tools and Manufacture, **44**(9), pp.879-887.

Bal, B., 2018. A study of different microstructural effects on the strain hardening behavior of Hadfield steel. International Journal of Steel Structures, **18**(1), pp.13-23.

Bal, B., Koyama, M., Canadinc, D., Gerstein, G., Maier, H.J. and Tsuzaki, K., 2018. On the utility of crystal plasticity modeling to uncover the individual roles of microdeformation mechanisms on the work hardening response of Fe-23Mn-0.5 C TWIP steel in the presence of hydrogen. Journal of Engineering Materials and Technology, **140**(3).

Bal, B., Sahin, I., Uzun, A. and Canadinc, D., 2016. A new venue toward predicting the role of hydrogen embrittlement on metallic materials. Metallurgical and Materials Transactions A, **47**(11), pp.5409-5422.

Calamaz, M., Coupard, D. and Girot, F., 2008. A new material model for 2D numerical simulation of serrated chip formation when machining titanium alloy Ti–6Al–4V. International Journal of Machine Tools and Manufacture, **48**(3-4), pp.275-288.

Da Silva, F.A.V., Denguir, L.A. and Outeiro, J.C., 2020. Residual stresses prediction in machining of Inconel 718 superalloy using a constitutive model considering the state of stress. Procedia CIRP, **87**, pp.527-532.

Dixit, U.S., Joshi, S.N. and Davim, J.P., 2011. Incorporation of material behavior in modeling of metal forming and machining processes: A review. Materials & Design, **32**(7), pp.3655-3670.

Eshelby, J., 2007. The determination of the elastic field of an ellipsoidal inclusion and related problems. Collected works of JD Eshelby.

Fitzpatrick, M.E., Fry, A.T., Holdway, P., Kandil, F.A., Shackleton, J. and Suominen, L., 2005. Determination of residual stresses by X-ray diffraction.

Grzesik, W., Niesłony, P. and Laskowski, P., 2017. Determination of material constitutive laws for Inconel 718 superalloy under different strain rates and working temperatures. Journal of Materials Engineering and Performance, **26**(12), pp.5705-5714.

Hua, J., Umbrello, D. and Shivpuri, R., 2006. Investigation of cutting conditions and cutting edge preparations for enhanced compressive subsurface residual stress in the hard turning of bearing steel. Journal of Materials Processing Technology, **171**(2), pp.180-187.

Jacobus, K., DeVor, R.E. and Kapoor, S.G., 2000. Machining-induced residual stress: experimentation and modeling. J. Manuf. Sci. Eng., **122**(1), pp.20-31.

Jawahir, I.S., Brinksmeier, E., M'saoubi, R., Aspinwall, D.K., Outeiro, J.C., Meyer, D., Umbrello, D. and Jayal, A.D., 2011. Surface integrity in material removal processes: Recent advances. CIRP annals, **60**(2), pp.603-626.

Johnson, G.R., 1983. A constitutive model and data for materials subjected to large strains, high strain rates, and high temperatures. Proc. 7th Inf. Sympo. Ballistics, pp.541-547.

Kocks, U.F., Tomé, C.N. and Wenk, H.R., 2000. Texture and anisotropy: preferred orientations in polycrystals and their effect on materials properties. Cambridge university press.

Kortabarria, A., Armentia, I. and Arrazola, P., 2016. Sensitivity analysis of material input data influence on machining induced residual stress prediction in Inconel 718. Simulation Modelling Practice and Theory, **63**, pp.47-57.

Lebensohn, R.A. and Tomé, C.N., 1993. A self-consistent anisotropic approach for the simulation of plastic deformation and texture development of polycrystals: application to zirconium alloys. Acta metallurgica et materialia, **41**(9), pp.2611-2624.

Liang, S.Y. and Su, J.C., 2007. Residual stress modeling in orthogonal machining. CIRP annals, **56**(1), pp.65-68.

Noyan, I.C. and Cohen, J.B., 2013. Residual stress: measurement by diffraction and interpretation. Springer.

Onal, O., Bal, B.U.R.A.K., Canadinc, D. and Akdari, E., 2015. Experimental and numerical evaluation of thickness reduction in steel plate heat exchangers. Journal of Engineering Materials and Technology, **137**(4), p.041008.

Onal, O., Bal, B., Toker, S.M., Mirzajanzadeh, M., Canadinc, D. and Maier, H.J., 2014. Microstructure-based modeling of the impact response of a

biomedical niobium–zirconium alloy. Journal of Materials Research, **29**(10), pp.1123-1134.

Outeiro, J.C., Pina, J.C., M'saoubi, R., Pusavec, F. and Jawahir, I.S., 2008. Analysis of residual stresses induced by dry turning of difficult-to-machine materials. CIRP annals, **57**(1), pp.77-80.

Outeiro, J.C., Umbrello, D. and M'saoubi, R., 2006. Experimental and numerical modelling of the residual stresses induced in orthogonal cutting of AISI 316L steel. International Journal of Machine Tools and Manufacture, **46**(14), pp.1786-1794.

Pawade, R.S., Joshi, S.S. and Brahmankar, P.K., 2008. Effect of machining parameters and cutting edge geometry on surface integrity of high-speed turned Inconel 718. International Journal of Machine Tools and Manufacture, **48**(1), pp.15-28.

Rahman, M., Seah, W.K.H. and Teo, T.T., 1997. The machinability of Inconel 718. Journal of materials processing technology, **63**(1-3), pp.199-204.

Rotella, G., Dillon Jr, O.W., Umbrello, D., Settineri, L. and Jawahir, I.S., 2013. Finite element modeling of microstructural changes in turning of AA7075-T651 alloy. Journal of Manufacturing Processes, **15**(1), pp.87-95.

Salio, M., Berruti, T. and De Poli, G., 2006. Prediction of residual stress distribution after turning in turbine disks. International Journal of Mechanical Sciences, **48**(9), pp.976-984.

Sharman, A.R.C., Hughes, J.I. and Ridgway, K., 2006. An analysis of the residual stresses generated in Inconel 718™ when turning. Journal of Materials Processing Technology, **173**(3), pp.359-367.

Sjöberg, T., Kajberg, J. and Oldenburg, M., 2018. Calibration and validation of three fracture criteria for alloy 718 subjected to high strain rates and elevated temperatures. European Journal of Mechanics-A/Solids, **71**, pp.34-50.

Strenkowski, J.S. and Carroll III, J.T., 1985. A finite element model of orthogonal metal cutting.

Sui, S., Li, Z., Zhong, C., Zhang, Q., Gasser, A., Chen, J., Chew, Y. and Bi, G., 2021. Laves phase tuning for enhancing high temperature mechanical property improvement in laser directed energy deposited Inconel 718. Composites Part B: Engineering, 215, p.108819.

Sui, S., Zhong, C., Chen, J., Gasser, A., Huang, W. and Schleifenbaum, J.H., 2018. Influence of solution heat treatment on microstructure and tensile properties of Inconel 718 formed by high-deposition-rate laser metal deposition. Journal of Alloys and Compounds, **740**, pp.389-399.

Tadano, Y., Kuroda, M. and Noguchi, H., 2012. Quantitative re-examination of Taylor model for FCC polycrystals. Computational materials science, **51**(1), pp.290-302.

Torrano, I., Barbero, O., Kortabarria, A. and Arrazola, P.J., 2011. Prediction of residual stresses in turning of Inconel 718. Trans Tech Publications Ltd., **223**, pp. 421-430).

Ulutan, D., Alaca, B.E. and Lazoglu, I., 2007. Analytical modelling of residual stresses in machining. Journal of Materials Processing Technology, **183**(1), pp.77-87.